Convective heat transfer in the Burgers-Rayleigh-Bénard system

Enrico Calzavarini* and Silvia C. Hirata
Université de Lille, Unité de Mécanique de Lille–J. Boussinesq, UML ULR 7512, F59000 Lille, France

(Received 23 January 2023; accepted 15 June 2023; published 30 June 2023)

The dynamics of heat transfer in a model system of Rayleigh-Bénard (RB) convection reduced to its essentials, here dubbed Burgers-Rayleigh-Bénard (BRB), is studied. The system is spatially one-dimensional, the flow field is compressible, and its evolution is described by the Burgers equation forced by an active temperature field. The BRB dynamics shares remarkable similarities with realistic RB thermal convection in higher spatial dimensions: (1) it has a supercritical pitchfork instability for the onset of convection which depends solely on the Rayleigh number (Ra) and not on the Prandlt number (Pr), occurring at the critical value $\mathrm{Ra}_c = (2\pi)^4$, (2) the convective regime is spatially organized in distinct boundary layers and bulk regions, and (3) the asymptotic high-Ra limit displays the Nusselt and Reynolds numbers scaling regime $\mathrm{Nu} = \sqrt{\mathrm{RaPr}}/4$ for $\mathrm{Pr} \ll 1$, $\mathrm{Nu} = \sqrt{\mathrm{Ra}}/(4\sqrt{\pi})$ for $\mathrm{Pr} \gg 1$, and $\mathrm{Re} = \sqrt{\mathrm{Ra}/\mathrm{Pr}}/\sqrt{12}$, thus making BRB the simplest wall-bounded convective system exhibiting the so-called ultimate regime of convection. These scaling laws, derived analytically through a matched asymptotic analysis are fully supported by the results of the accompanying numerical simulations. A major difference with realistic natural convection is the absence of turbulence. The BRB dynamics is stationary at any Ra number above the onset of convection. This feature results from a nonlinear saturation mechanism whose existence is grasped by means of a two-mode truncated equation system and via a stability analysis of the convective regime.

DOI: 10.1103/PhysRevFluids.8.063502

I. INTRODUCTION

Thought experiments, toy models, and low-dimensional representations are keys to scientific thinking and allow insight into the complex physics of many real systems. In fluid-dynamics research, reduced models obtained, e.g., via expansion and truncations of the original dynamical equations have been used to conceptualize and to understand, for instance, the chaotic dynamics of flows (Lorenz system [1]) or the physics of energy cascade in developed turbulence (shell models [2,3]). In this study we focus on the problem of thermal convection and, in the spirit of the one-dimensional (1D) toy model for granular media introduced by Du, Li, and Kadanoff [4,5], we introduce a stripped-down mock-up of the classical Rayleigh-Bénard (RB) system [6].

The RB has been extensively studied either in its spatial three-dimensional (3D) or in its two-dimensional (2D) version [7,8]. We are not aware of any study of the system in one dimension. This is after all quite understandable, since in one dimension the incompressibility condition for the flow does not hold, and one expects a rather different physical behavior. This is indeed already the case for the 1D version of the Navier-Stokes equation, i.e., the Burgers equation [9]. It is well known that the Burgers equation does not display a turbulent behavior, because it can be recast in terms of a diffusion equation via the Hopf-Cole transformation [10,11]. However, a stochastically forced

*enrico.calzavarini@univ-lille.fr

Burgers equation does produce a special kind of turbulence, dubbed Burgulence [12], that has drawn the attention of recent research [13].

We show in this study that a 1D deterministically forced version of the RB system that we dub the Burgers-Rayleigh-Bénard (BRB) system can be defined. Interestingly, this system possesses a certain number of similarities with thermal convection in higher spatial dimensions: it has a supercritical linear instability for the onset of convection, the convective regime is spatially organized in distinct boundary layers and bulk regions, and the asymptotic high-Ra limit displays the so-called ultimate Nusselt and Reynolds number scalings [8], although it lacks any turbulent behavior. It also admits shocklike solutions that are peculiar to the Burgers dynamics.

The article is organized as follows. We first define the BRB system; next we examine its most relevant symmetries and its global properties. In particular, we introduce the definition of the Nusselt and Reynolds numbers, which are the two global response parameters of the system. Second, we perform a theoretical analysis on the system dynamics, focusing on the calculation of the linear instability threshold for convection, on the subsequent nonlinear saturation mechanism, and on a derivation of a steady matched asymptotic solution for the very intense convection state. Third, we push forward the analysis by means of a numerical approach. In particular we show that the system is stationary at all Rayleigh numbers; this is first revealed empirically, then verified by means of numerically based stability analysis. We then show that the Nusselt and Reynolds numbers asymptotically approach the ultimate state of thermal convection, this in both their Rayleigh and Prandtl number dependencies. Finally, we discuss the implications of our findings and possible perspectives.

II. THE BURGERS-RAYLEIGH-BÉNARD MODEL SYSTEM

A. Equations of motion

We study the spatiotemporal evolution of a single-component velocity $W(Z,\tau)$ and temperature $T(Z,\tau)$ fields in a 1D domain $Z \in [0,H]$, described by the coupled system of differential equations

$$W_\tau + W\, W_Z = \nu\, W_{ZZ} + \beta g (T - T_c), \tag{1}$$

$$T_\tau + W\, T_Z = \kappa\, T_{ZZ}, \tag{2}$$

with Dirichlet boundary conditions

$$W = 0,\ T = \tfrac{\Delta}{2} \quad \text{in } Z = 0 \text{ (bottom)}, \tag{3}$$

$$W = 0,\ T = -\tfrac{\Delta}{2} \quad \text{in } Z = H \text{ (top)}, \tag{4}$$

where ν and κ denote, respectively, the viscosity and thermal diffusivity, β the thermal expansion coefficient, g the gravitational acceleration intensity, and T_c the linear profile given by $T_c(Z) = -(\Delta/H)Z + \Delta/2$, which is also said conductive because it represents a solution for the temperature field when $W = 0$ in all the domain. Furthermore, to keep the similarity with realistic RB convection we adopt the additional constraint that the global value of velocity and temperature fields are null,

$$\int_0^H W\, dZ = \int_0^H T\, dZ = 0 \ \text{ (no-zero mode condition)}. \tag{5}$$

This prevents the possibility for the system to acquire a vertical mean flow and to heat up or cool off. We will comment later on the consequence of this constraint.

As we have already mentioned, the above model constitutes an oversimplified representation of the Rayleigh-Bénard system. It can be loosely obtained from the Navier-Stokes-Boussinesq set of equations for the 3D velocity $\mathbf{U} = (U, V, W)$ and temperature T, by assuming that (1) the vertical component of the velocity, W, and the temperature depend only on the vertical direction, Z, (2) by removing the hydrodynamic pressure field, and (3) by expressing the buoyancy force as proportional to the temperature deviation from the local conductive temperature profile. With the

above assumptions, the equations for T and W decouple from the ones for horizontal components U, V and can be treated separately. As a consequence the vertical velocity gradient W_Z becomes unconstrained and the corresponding unidimensional velocity field is compressible. We stress that the BRB model cannot be regarded as a low-dimensional mean-field form of the Boussinesq system, nor a model of convection in compressible gases (where the continuity equation would have a different form). However, we believe that despite its incompleteness this model is useful to get an insight into what does or does not occur in the realistic system.

Equations (1) and (2) can be made dimensionless by means of the linear size of the domain (or height H), the free-fall velocity $U_f = \sqrt{\beta g H \Delta}$, and the global temperature gap Δ (i.e., the difference between the top temperature and the bottom one). This leads to the two control parameters in the system: the Rayleigh number $\mathrm{Ra} = (U_f H)^2/(\nu\kappa)$ and the Prandtl number $\mathrm{Pr} = \nu/\kappa$. With these choices the equations can be conveniently rewritten in terms of the velocity, $w = W/U_f$, and the temperature deviation from the conductive profile, $\theta(z,t) = [T(Z,\tau) - T_c(Z)]/\Delta$, as

$$w_t + w\, w_z = \sqrt{\frac{\mathrm{Pr}}{\mathrm{Ra}}}\, w_{zz} + \theta, \tag{6}$$

$$\theta_t + w\, \theta_z = \frac{1}{\sqrt{\mathrm{PrRa}}}\, \theta_{zz} + w, \tag{7}$$

with $w = \theta = 0 \quad \text{in} \quad z = 0$ and $z = 1$ and $\langle w \rangle = \langle \theta \rangle = 0$, where $\langle \cdots \rangle = \int_0^1 \cdots dz$ is the spatial average (all lower-case letters denote dimensionless variables). Equation (6) is the 1D forced Burgers equation, which is coupled to the advection-diffusion equation for a scalar field (7), which is in turn forced by w.

B. Symmetries

The system (6)–(7) enjoys a series of symmetries which greatly affect its dynamics. We describe them in detail in this section. To begin, we note that when $\mathrm{Pr} = 1$, $\theta = w$ is a permitted solution of the BRB model system.

Second, the set of equations (6)–(7) is invariant with respect to the transformation $(z, \theta) \to (1 - z, -\theta)$, which also implies $w \to -w$ because by definition $w = dz/dt$. This means that if the couple $\theta(t, z)$, $w(t, z)$ indicates a solution of the equations, then $-\theta(t, 1 - z)$, $-w(t, 1 - z)$ is also a solution. Combining this with the condition $\langle w \rangle = \langle \theta \rangle = 0$, it entails that both θ and w are odd functions with respect to $z = 1/2$, and so $\theta(z = 1/2) = w(z = 1/2) = 0$.

A third symmetry is the following:

$$z \to \begin{cases} z + 1/2 \text{ if } z \leqslant 1/2 \\ z - 1/2 \text{ if } z > 1/2 \end{cases} \quad \text{or} \quad z \to z + \mathrm{sign}\left(\frac{1}{2} - z\right)\frac{1}{2}. \tag{8}$$

It corresponds to swapping the spatial interval $[0, 1/2]$ with the one $[1/2, 1]$. As shown in the sketch in Figs. 1(a) and 1(b) this symmetry transforms what we call a "boundary-layer"-type solution to a "shock"-type solution (more on this later). In other words, due to the zero boundary conditions and to the second symmetry, the functions $w(z)$ and $\theta(z)$ can be seen as periodic odd functions. This means that adding a phase of half the period is still a solution of the system. Equivalently one can say that $z \to z + 1/2$ is a symmetry of the system.

A fourth remarkable symmetry of the system is the following: let's call $w(t, z; \mathrm{Ra}, \mathrm{Pr})$, $\theta(t, z; \mathrm{Ra}, \mathrm{Pr})$ the solution of the system for a given value of the parameters Ra, Pr. The system is then invariant with respect to the transformation:

$$w(t, z; \mathrm{Ra}, \mathrm{Pr}) \to w\left(t, 2nz; \frac{\mathrm{Ra}}{2n}, \mathrm{Pr}\right)/(2n), \tag{9}$$

$$\theta(t, z; \mathrm{Ra}, \mathrm{Pr}) \to \theta\left(t, 2nz; \frac{\mathrm{Ra}}{2n}, \mathrm{Pr}\right)/(2n), \tag{10}$$

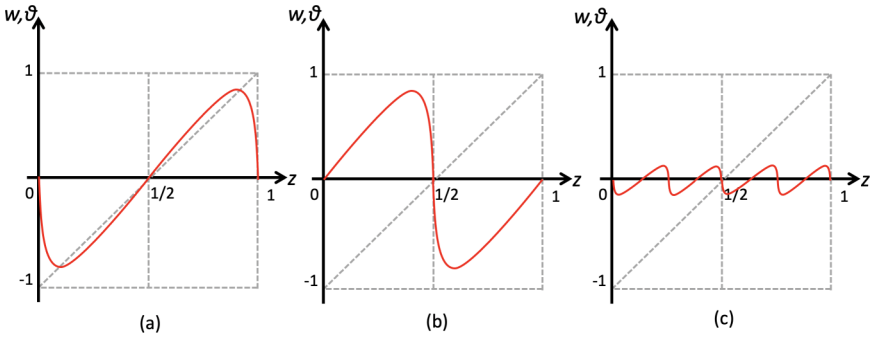

FIG. 1. Symmetries of the system of equations: (a) odd symmetry of w and θ with respect to the position $z = 1/2$; (b) swap symmetry with resect to the system midpoint (8); (c) rescaling transformation [(9)–(10)] with $n = 1$.

where n is a positive integer number. This "rescaling transformation" symmetry is illustrated in Fig. 1(c) for the case $n = 1$.

C. Global response parameters: Nusselt and Reynolds numbers

To derive the expression for the global heat flux it is convenient to resort to the dimensional notation. The temperature equation (2) in conservative form reads $T_\tau + (J_T)_Z = 0$, where

$$J_T(Z,\tau) = WT - \kappa T_Z - \int_0^Z TW_{Z'}\, dZ' \tag{11}$$

is the local and instantaneous heat flux at position Z and time τ. Averaging the conservative form equation over time (here denoted as an overline) and assuming a steady state gives the expression of the mean global heat flux:

$$\overline{J_T}(Z) = \overline{WT} - \kappa \overline{T}_Z - \int_0^Z \overline{TW_{Z'}}\, dZ' = \text{const.} \tag{12}$$

The integral term in the above expression, which is absent in the mean heat flux of the RB system, is a consequence of the compressibility of the velocity field. The mean Nusselt number is defined by adimensionalizing the mean global heat flux with respect to the conductive heat flux (i.e., the state where $W = 0$ and $T = T_c$):

$$\text{Nu} \equiv \frac{\overline{J_T}}{J_{T_c}} = \text{const.} \tag{13}$$

We observe that by plugging into the above expression the dimensionless temperature fluctuation θ, and evaluating the expression in either $z = 0$ or $z = 1$, gives the following equivalent expressions for Nu:

$$\text{Nu} = 1 - \overline{\theta}_z(0) = 1 - \overline{\theta}_z(1). \tag{14}$$

One can remark that this same expression for Nu is obtained in the RB flow ruled by the Boussinesq system of equations. On the contrary, if one considers the spatial average of Nu [spatial average of Eq. (13)] one gets

$$\text{Nu} = 1 + \sqrt{\text{PrRa}}\left(\langle \overline{w\theta} \rangle - \left\langle \int_0^z (\overline{\theta w_{z'}} + \overline{w}) dz' \right\rangle \right), \tag{15}$$

which is different from the RB expression by the appearance of the integral term on the r.h.s., which originates, as already mentioned, by the flow compressibility. The volume-averaged expression of

the Nusselt number is convenient for numerical calculations, as it is less affected by discretization and numerical errors (we will use this expression in the numerical calculations presented in this article).

Finally, we note that the Reynolds number defined as a system response parameter is here:

$$\mathrm{Re} \equiv \frac{\overline{\langle W^2 \rangle}^{1/2} H}{\nu} = \sqrt{\frac{\mathrm{Ra}}{\mathrm{Pr}}}\, \overline{\langle w^2 \rangle}^{1/2}. \tag{16}$$

III. THE BRB DYNAMICS: THEORETICAL ANALYSIS

This section presents some notable analytical results on the dynamics of the BRB model system. First, we perform the linear stability analysis to determine the transition from the conductive to the convective state. Second, we address the nonlinear saturation mechanism that is responsible for the stabilization of the flow after the inception of convection. Third, by means of a standard matched asymptotic (*ma*) analysis, we solve the BRB system of equations in a steady condition in the limit of large Ra numbers. Finally, based on the *ma* solution we derive the asymptotic-in-Rayleigh scaling laws for the Nusselt and Reynolds numbers.

A. Onset of convection

The linearization of the system (6)–(7) with respect to w and θ satisfies solutions of the form

$$w = \Sigma_{n=1}^{\infty} w_n e^{\sigma_n t} \sin(nkz), \quad \theta = \Sigma_{n=1}^{\infty} \theta_n e^{\sigma_n t} \sin(nkz), \tag{17}$$

where $k = 2\pi$ and n is an integer value, and with the growth rate

$$\sigma_n = \frac{\sqrt{(\mathrm{Pr}+1)^2 (nk)^4 + 4\mathrm{Pr}[\mathrm{Ra} - (nk)^4]} - (\mathrm{Pr}+1)(nk)^2}{2\sqrt{\mathrm{RaPr}}}. \tag{18}$$

Therefore, for $\mathrm{Ra} > \mathrm{Ra}_c = k^4 = (2\pi)^4 \simeq 1558$, and at any Pr value the system becomes linearly unstable ($\sigma_1 > 0$). The critical Rayleigh number happens to be the same as in the 3D three-periodic homogeneous Rayleigh-Bénard system [14,15] although in that case the perturbation form is different as it depends only on the horizontal coordinates. We observe that the relative amplitude of the velocity and temperature field is $w_1/\theta_1 = (\sigma_1 + k^2/\sqrt{\mathrm{PrRa}})$, and this implies that $w_1 = \theta_1$ for $\mathrm{Pr} = 1$. This prediction will be verified in Sec. IV by means of a numerical simulation starting from a tiny white noise perturbation on w and θ fields (see also Fig. 6).

The described exponentially growing solution is eventually saturated by the presence of the nonlinear terms, as we discuss in the next section.

B. Nonlinear saturation mechanism

Similarly to what occurs in a 3D RB system in slightly supercritical conditions ($\mathrm{Ra} \gtrsim \mathrm{Ra}_c$) the exponential growth rate of the perturbation rapidly saturates into a convective steady state. This phenomenology can be promptly explained for the BRB at $\mathrm{Pr} = 1$ by means of a two-mode Galerkin expansion, which we detail in the following. We assume

$$w(z,t) = \Sigma_{n=1,2} A_n(t) \sin(nkz), \quad \theta(z,t) = \Sigma_{n=1,2} B_n(t) \sin(nkz). \tag{19}$$

Upon its substitution into the equations of motion, retaining only terms in $\sin(kz)$ and $\sin(2kz)$, we obtain the first-order differential system for the evolution of the amplitudes of the four considered modes:

$$\dot{A_1} = \frac{\mathrm{Ra}_c^{1/4}}{2} A_1 A_2 - \sqrt{\frac{\mathrm{Ra}_c}{\mathrm{Ra/Pr}}} A_1 + B_1, \tag{20}$$

$$\dot{A_2} = -\frac{\mathrm{Ra}_c^{1/4}}{2}A_1^2 - 4\sqrt{\frac{\mathrm{Ra}_c}{\mathrm{Ra/Pr}}}A_2 + B_2, \tag{21}$$

$$\dot{B_1} = \frac{\mathrm{Ra}_c^{1/4}}{2}(2A_1B_2 - A_2B_1) - \sqrt{\frac{\mathrm{Ra}_c}{\mathrm{RaPr}}}B_1 + A_1, \tag{22}$$

$$\dot{B_2} = -\frac{\mathrm{Ra}_c^{1/4}}{2}A_1B_1 - 4\sqrt{\frac{\mathrm{Ra}_c}{\mathrm{RaPr}}}B_2 + A_2, \tag{23}$$

where we have taken into account that $\mathrm{Ra}_c = k^4$. Such a system can not be solved analytically; however, that is possible for the special case $\mathrm{Pr} = 1$. In this condition the equations for A_i and B_i become identical, hence the differential system reduces to a 2D one:

$$\dot{A_1} = \sigma_1 A_1 + \frac{\mathrm{Ra}_c^{1/4}}{2}A_1A_2, \tag{24}$$

$$\dot{A_2} = \sigma_2 A_2 - \frac{\mathrm{Ra}_c^{1/4}}{2}A_1^2, \tag{25}$$

with $\sigma_1 = 1 - \sqrt{\mathrm{Ra}_c/\mathrm{Ra}} > 0$ and $\sigma_2 = 1 - 4\sqrt{\mathrm{Ra}_c/\mathrm{Ra}} < 0$ for $\mathrm{Ra}_c < \mathrm{Ra} < 16\mathrm{Ra}_c$. As the characteristic timescale of the second mode $\tau_2 = |\sigma_2|^{-1}$ is smaller than the characteristic time of the first mode $\tau_1 = |\sigma_1|^{-1}$, we can perform a so-called adiabatic elimination and take $\dot{A_2} \approx 0$ in the vicinity of the bifurcation threshold. By doing so, we obtain the following Landau equation [16] for the evolution of the amplitude A_1:

$$\dot{A_1} = \sigma_1 A1 - \gamma A_1^3 \tag{26}$$

with $\gamma = \frac{\sqrt{\mathrm{Ra}_c}}{4(4\sqrt{\frac{\mathrm{Ra}_c}{\mathrm{Ra}}}-1)}$. Equation (26) admits three steady solutions:

$$A_1^{ss} = 0 \ \text{(conductive state)}, \tag{27}$$

$$A_1^{ss} = \pm\sqrt{\sigma_1/\gamma} \ \text{(two convective states)}. \tag{28}$$

Assuming the perturbation expansion $A_1(t) = A_1^{ss} + \varepsilon A_{1p}(t) + O(\varepsilon^2)$, the amplitude equation at order $O(\varepsilon)$ writes

$$\dot{A}_{1p} = A_{1p}(t)\left[\sigma_1 - 3\gamma\left(A_1^{ss}\right)^2\right]. \tag{29}$$

A solution of the linear and homogeneous equation above can be written as $A_{1p}(t) = A_{1p}(0)\exp(-i\omega t)$, which leads to

$$\sigma_1 - 3\gamma\left(A_1^{ss}\right)^2 + i\omega = 0. \tag{30}$$

Since all the coefficients are real and $\omega = \omega_R + i\omega_I$, we get $\omega_R = 0$ (meaning that solutions are stationary) and $\omega_I = \sigma_1 - 3\gamma(A_1^{ss})^2$. Hence, the growth rates of the trivial (27) and nontrivial (28) steady states are $\omega_I = \sigma_1$ and $\omega_I = -2\sigma_1$ respectively. Therefore, for $\mathrm{Ra} < \mathrm{Ra}_c$ the trivial conductive solution is stable, whereas for $\mathrm{Ra} > \mathrm{Ra}_c$ the nontrivial convective solutions are the ones to be stable. This corresponds to a supercritical pitchfork bifurcation, as illustrated in Fig. 2.

The multiplicity of the above convective solutions is a consequence of the swap symmetry mentioned in the previous section, which in the case of a sinusoidal profile takes the form $\sin(nkz) \to (-1)^n \sin(nkz)$ for integers n. In the two-mode expansion it therefore affects only the mode A_1. This produces a change from a solution with sharp variations at the boundaries, which we can denote as "boundary layer"-type solution, to one with a sharp transition in the bulk of the domain, which we call "shock"-type solution. While the boundary layer-type solution is analogous to the vertical flow profile observed in the RB system, the shock-type solution has no corresponding in 2D or 3D convective systems. For this reason, in our analysis we will mainly focus on the

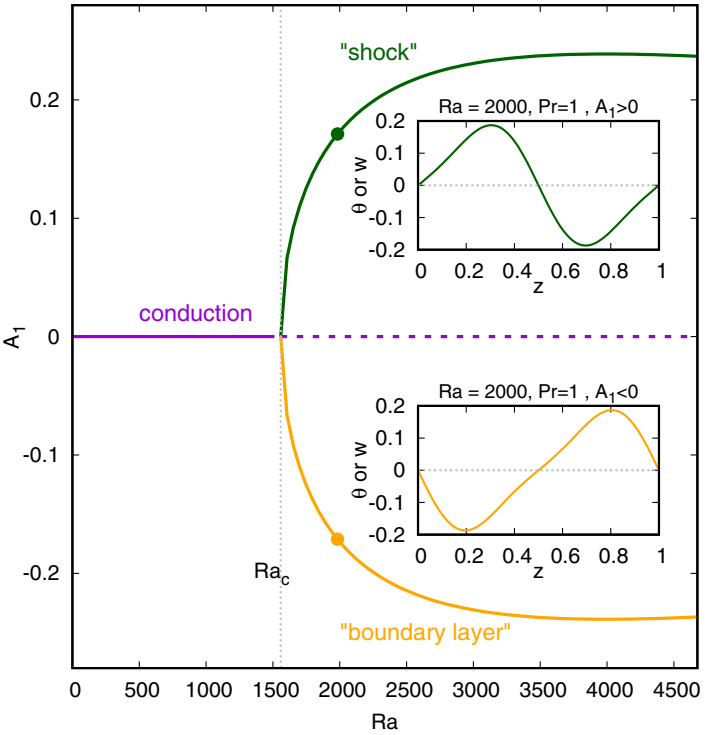

FIG. 2. Steady solution of the amplitude A_1 of the two-mode truncated system as a function of the control parameter Ra, as given in Eqs. (27) and (28). The graph has a typical structure of a supercritical pitchfork bifurcation; solid lines denote stable branches, while the dotted one denotes the unstable branch. We indicate as "conduction" the solution corresponding to $A_1 = 0$ (and $A_2 = 0$ too), with the "shock"-type solution the one presenting a sharp variation on the bulk of the system, which corresponds to the case $A_1 > 0$, and finally with "boundary layer"-type, the one where the variation occurs close to the boundaries ($A_1 < 0$ in this case). The insets show the complete steady two-mode solutions for $\theta(z)$ or $w(z)$ of the shock and boundary layer types for the case Ra $= 2000$, marked with colored circles on the main panels.

former kind of solution. The temperature or velocity spatial profiles corresponding to the complete convective steady solutions of (24)–(25), i.e., the two-mode truncated series (19) with

$$A_1 = \pm\sqrt{\sigma_1/\gamma} = \frac{\pm 2}{\mathrm{Ra}_c^{1/4}}\left(1-\sqrt{\frac{\mathrm{Ra}_c}{\mathrm{Ra}}}\right)^{\frac{1}{2}}\left(4\sqrt{\frac{\mathrm{Ra}_c}{\mathrm{Ra}}}-1\right)^{\frac{1}{2}}, \tag{31}$$

$$A_2 = -2\sigma_1/\mathrm{Ra}_c^{1/4} = \frac{-2}{\mathrm{Ra}_c^{1/4}}\left(1-\sqrt{\frac{\mathrm{Ra}_c}{\mathrm{Ra}}}\right) \tag{32}$$

are traced in Fig. 2 (insets) [17].

The above convective solutions allows to estimate the Nusselt number near to the onset, as

$$\mathrm{Nu} = 1 - 2\pi(A_1 + 2A_2). \tag{33}$$

They also imply that

$$\langle w^2\rangle = \langle\theta^2\rangle = \langle w\theta\rangle = \frac{1}{2}\left(A_1^2 + A_2^2\right) = \frac{6}{\sqrt{\mathrm{Ra}}}\left(1-\sqrt{\frac{\mathrm{Ra}_c}{\mathrm{Ra}}}\right), \tag{34}$$

so the Reynolds number becomes

$$\mathrm{Re} = \sqrt{6(\sqrt{\mathrm{Ra}} - \sqrt{\mathrm{Ra}_c})}. \tag{35}$$

These predictions will be tested in Sec. IV by means of direct numerical simulations.

Finally, we wish to comment on the role of the no-zero mode condition, $\langle w \rangle = \langle \theta \rangle = 0$, introduced in our model system. The removal of this condition allows for an anticipated onset of convection at $\mathrm{Ra}_c = \pi^4$ (16 times smaller than in the present case). It also permits nonodd solutions characterized by a single boundary layer on one of the sides of the domain. By virtue of the system symmetries, these solutions are trivially linked to the ones described above: their period and their amplitude are doubled, but all scaling properties remain identical.

C. Large-Ra asymptotic dynamics

What happens to the system dynamics at large Ra? Does it stay stationary, or rather does it become time dependent, and possibly chaotic and turbulent? Replying to these questions on the basis of a theoretical analysis is challenging. We will try to reply to this question with the aid of numerical simulations, in Sec IV. However, it is possible to derive a steady solution of (6)–(7) in the limit of large Ra and at any Pr, by means of the standard technique of matched asymptotic expansion. In the following we detail the derivation of such a remarkable solution, and we will then use it to give a prediction for the Nusselt and Reynolds scaling in the asymptotically large Ra regime. The numerical simulations, described in Sec IV, will prove that the steady *ma* solution describes strikingly well the real behavior of the BRB system.

1. Approximate stationary solution with matched asymptotic expansion

The use of matched asymptotics to describe the structure of shocks in the Burgers equation at very small viscosities is a classical approach [18]. This technique has been applied in several studies to estimate the contribution of shocks to the anomalous dissipation of kinetic energy [19] and to the energy spectrum of solutions [20], to propose closures for statistical theories of Burgers' turbulence [21], and more recently to explain the spontaneous stochasticity of Lagrangian trajectories in the Burgers equation [22].

Here we look for a solution of Eqs. (6)–(7) under the assumption that both $\frac{\sqrt{\mathrm{Pr}}}{\sqrt{\mathrm{Ra}}}$ and $\frac{1}{\sqrt{\mathrm{RaPr}}}$ are small parameters (or equivalently $\mathrm{Ra}^{-1} \ll \mathrm{Pr} \ll \mathrm{Ra}$). First, we consider the solution of the system far from boundaries, denoted as the *outer* solution. In this region the dissipative terms are negligible, because they multiply the above mentioned small parameters, hence the system reduces to

$$w\, w_z = \theta, \tag{36}$$

$$w\, \theta_z = w. \tag{37}$$

From the second equation we get $\theta_{\mathrm{out}} = z + c_1$, which is then plugged into the first equation leading to $w w_z = z + c_1$, which admits the solution $w_{\mathrm{out}} = \sqrt{z^2 + 2c_1 z + c_2}$. By using the condition that the solution should be an odd function in the domain [i.e., $w(1/2) = \theta(1/2) = 0$] we determine the constants $c_1 = -1/2$, $c_2 = 1/4$ and so $w_{\mathrm{out}} = \theta_{\mathrm{out}} = z - 1/2$.

Second, we consider the solution near to a boundary, denoted as *inner* solution (we choose here the boundary close to $z = 0$). In this region the application of standard least degeneracy principle [23] leads to the system

$$w\, w_z = \frac{\sqrt{\mathrm{Pr}}}{\sqrt{\mathrm{Ra}}}\, w_{zz}, \tag{38}$$

$$w\, \theta_z = \frac{1}{\sqrt{\mathrm{PrRa}}}\, \theta_{zz}. \tag{39}$$

Here one first solves the equation for w. This leads to $w_{\rm in} = -a\tanh\left(a\sqrt{\frac{\rm Ra}{\rm Pr}}\,z/2\right)$ where we have adopted the boundary condition in $w(0) = 0$. The constant a can be determined by matching the inner and outer solutions for w, $\lim_{z\to\infty} w_{\rm in} = \lim_{z\to 0} w_{\rm out}$: $-a = -1/2$, so $a = 1/2$:

$$w_{\rm in} = -\frac{1}{2}\tanh\left(\sqrt{\frac{\rm Ra}{\rm Pr}}\,\frac{z}{4}\right). \tag{40}$$

By substituting now the inner solution $w_{\rm in}$ in the equation for θ we obtain

$$-\frac{1}{2}\tanh\left(\sqrt{\frac{\rm Ra}{\rm Pr}}\,\frac{z}{4}\right)\theta_z = \tfrac{1}{\sqrt{\rm PrRa}}\,\theta_{zz}, \tag{41}$$

which can be rewritten as

$$-\frac{1}{2}\sqrt{\rm PrRa}\tanh\left(\sqrt{\frac{\rm Ra}{\rm Pr}}\,\frac{z}{4}\right) = \frac{d}{dz}\log\theta_z \tag{42}$$

and integrated to

$$\log\left[\cosh\left(\sqrt{\frac{\rm Ra}{\rm Pr}}\,\frac{z}{4}\right)\right]^{-2\rm Pr} = \log\theta_z + \log K, \tag{43}$$

where $\log K$ is a constant, hence removing the log:

$$\left[\cosh\left(\sqrt{\frac{\rm Ra}{\rm Pr}}\,\frac{z}{4}\right)\right]^{-2\rm Pr} = K\theta_z. \tag{44}$$

This can be integrated in the interval $[0, z]$

$$\theta(z) - \theta(0) = \frac{1}{K}\int_0^z\left[\cosh\left(\sqrt{\frac{\rm Ra}{\rm Pr}}\,\frac{z'}{4}\right)\right]^{-2\rm Pr} dz'. \tag{45}$$

We now apply the boundary condition $\theta(0) = 0$, while the value of K is obtained by matching the inner and outer solutions for θ, $\lim_{z\to\infty}\theta_{\rm in} = \lim_{z\to 0}\theta_{\rm out}$: $-\frac{1}{2} = \frac{1}{K}\lim_{z\to\infty}\int_0^z[\cosh(\sqrt{\frac{\rm Ra}{\rm Pr}}\,\frac{z'}{4})]^{-2\rm Pr}dz'$. It follows:

$$\theta_{\rm in}(z) = -\frac{1}{2}\frac{\int_0^z\left[\cosh\left(\sqrt{\frac{\rm Ra}{\rm Pr}}\,\frac{z'}{4}\right)\right]^{-2\rm Pr}dz'}{\int_0^\infty\left[\cosh\left(\sqrt{\frac{\rm Ra}{\rm Pr}}\,\frac{z'}{4}\right)\right]^{-2\rm Pr}dz'}. \tag{46}$$

The complete perturbative solution is obtained by summing up the inner and the outer solution and by subtracting their overlap, $w_{ma}(z) = w_{\rm in}(z) + w_{outer}(z) - w_{overlap}$, where $w_{overlap} = \lim_{z\to\infty} w_{\rm in} = \lim_{z\to 0} w_{\rm out} = -\frac{1}{2}$. This leads to the final expression for the matched asymptotic solution:

$$w_{ma}(z) = z - \frac{1}{2}\tanh\left(\sqrt{\frac{\rm Ra}{\rm Pr}}\,\frac{z}{4}\right), \tag{47}$$

$$\theta_{ma}(z) = z - \frac{1}{2}\frac{\int_0^z\left[\cosh\left(\sqrt{\frac{\rm Ra}{\rm Pr}}\,\frac{z'}{4}\right)\right]^{-2\rm Pr}dz'}{\int_0^\infty\left[\cosh\left(\sqrt{\frac{\rm Ra}{\rm Pr}}\,\frac{z'}{4}\right)\right]^{-2\rm Pr}dz'}. \tag{48}$$

We note that if $\rm Pr = 1$ the solutions take the simpler form

$$w_{ma}(z) = \theta_{ma}(z) = z - \tfrac{1}{2}\tanh\left(\sqrt{\rm Ra}\,\frac{z}{4}\right). \tag{49}$$

The solution (49) for $\mathrm{Pr} = 1$ coincides with the shock solution derived by Saffman [24] for the randomly forced Burgers equation in the limit of $t \to +\infty$ and large Re (when $\sqrt{\mathrm{Ra}}$ is replaced by Re); see also [25] for a recent discussion.

Remark that the matched asymptotic solutions (47) and (48) are valid only in the interval $z \in [0, 1/2]$, but they can be applied to the interval $z \in [1/2, 1]$ with the transformation $z \to z - 1$. This at the price of accepting a discontinuity in the origin, because, e.g., for the velocity $w_{ma}(z = 1/2) = \varepsilon \neq 0$. However, such a discontinuity goes as $2\varepsilon = 1 - \tanh(\sqrt{\frac{\mathrm{Ra}}{\mathrm{Pr}}}\frac{1}{8})$, and therefore it vanishes asymptotically with Ra. We also note that the perturbative solution is not an exact solution of the original system. However, it is asymptotically correct. This can be seen by plugging it into the stationary equations and considering the $\mathrm{Ra} \to \infty$ limit of the residuals

$$\lim_{\mathrm{Ra}\to\infty} w_{ma} w_{ma,z} - \frac{\sqrt{\mathrm{Pr}}}{\sqrt{\mathrm{Ra}}}\, w_{ma,zz} - \theta_{ma} = 0,$$
$$\lim_{\mathrm{Ra}\to\infty} w_{ma} \theta_{ma,z} - \frac{1}{\sqrt{\mathrm{PrRa}}}\, \theta_{ma,zz} - w_{ma} = 0.$$

Another observation is in order about the the shape of the solution. By choosing that the internal solution occurs at $z = 0$, we have implicitly selected the boundary-layer type of the solution. A different, equally admissible choice is to place the inner solution close to $z = 1/2$, and this leads to a shock-type solution. One can trivially go from the former type of solution to the latter by applying the third symmetry transformation (8) discussed in Sec. II B. We observe that these two types of solutions are characterized by the same Reynolds number, as $\mathrm{Re} \sim \langle w^2 \rangle^{1/2}$, while they differ for the Nusselt number, because $\mathrm{Nu} = 1 - \theta_z(0)$. The latter observation implies that while boundary layer (BL)-type solutions are characterized by an increasing Nu as $\mathrm{Ra} \to \infty$, in the shock-type solution the Nusselt number vanishes (leading to a perfectly insulating system for $\mathrm{Ra} \to \infty$). As we mentioned before, although these two convective states are equally probable, we will limit our considerations to the case of a BL-type solution, as it offers a better analogy with the dynamics of the realistic RB system which motivates this study.

D. Upper bounds and asymptotic scalings for the Nusselt and Reynolds numbers

The matched asymptotic solution allows us to promptly compute asymptotic expressions for all global quantities in the system; we focus here on the two main output observables of the BRB system, the Nusselt and the Reynolds numbers.

1. Nusselt number

We evaluate $\mathrm{Nu} = 1 - \theta_{ma,z}(0)$. In the general Pr case, by using (48) we get

$$\mathrm{Nu} = \frac{1}{2\int_0^\infty \left[\cosh\left(\sqrt{\frac{\mathrm{Ra}}{\mathrm{Pr}}}\,\frac{z'}{4}\right)\right]^{-2\mathrm{Pr}} dz'}. \tag{50}$$

First, let us note that the Ra dependence can be factorized by introducing the auxiliary variable $\tilde{z} = \sqrt{\mathrm{Ra}}\, z'$ in the integral, so

$$\mathrm{Nu} = \frac{\sqrt{\mathrm{Ra}}}{2\int_0^\infty \left[\cosh\left(\frac{\tilde{z}}{4\sqrt{\mathrm{Pr}}}\right)\right]^{-2\mathrm{Pr}} d\tilde{z}}. \tag{51}$$

Because the denominator depends only on Pr it is therefore clear that the scaling $\mathrm{Nu} \sim \sqrt{\mathrm{Ra}}$ is to be expected asymptotically in Ra for any Pr.

We now focus on the Pr dependence. Using the property $e^x/2 \leqslant \cosh x \leqslant e^x$ for $x > 0$, one can write

$$\frac{2^{2\mathrm{Pr}+1}}{\sqrt{\mathrm{Pr}}} \geqslant \int_0^\infty \left[\cosh\left(\frac{\tilde{z}}{4\sqrt{\mathrm{Pr}}}\right)\right]^{-2\mathrm{Pr}} d\tilde{z} \geqslant \frac{2}{\sqrt{\mathrm{Pr}}},$$

and finally by using (51),

$$\frac{\sqrt{\mathrm{RaPr}}}{4^{\mathrm{Pr}+1}} \leqslant \mathrm{Nu} \leqslant \frac{\sqrt{\mathrm{RaPr}}}{4}.$$

This bounding relation is relevant in the limit of small Pr, because $4^{\mathrm{Pr}} \to 1$, leading to the scaling law

$$\mathrm{Nu} \simeq \frac{\sqrt{\mathrm{RaPr}}}{4} \quad (\mathrm{Pr\ small}). \tag{52}$$

In the limit of large Pr as $[\cosh(\frac{\tilde{z}}{4\sqrt{\mathrm{Pr}}})]^{-2\mathrm{Pr}} \to e^{-(\frac{\tilde{z}}{4})^2}$ and using (51) one obtains

$$\mathrm{Nu} = \frac{\sqrt{\mathrm{Ra}}}{4\sqrt{\pi}} \quad (\mathrm{Pr} \to \infty), \tag{53}$$

which is an expression that does remarkably not depend on the Pr value. It is worth observing that the saturation of the Nu number for large Pr values (53) is a feature also observed in the realistic RB system (see, e.g., [26], Fig. 5). Finally, for the intermediate case, $\mathrm{Pr} = 1$, taking advantage of the simpler form of the matched asymptotic solution (49), one can exactly derive

$$\mathrm{Nu} = \frac{\sqrt{\mathrm{Ra}}}{8} \quad (\mathrm{Pr} = 1). \tag{54}$$

2. Reynolds number

We now turn the attention to the Reynolds number. Asymptotically in Ra we observe that the *ma* velocity solution approaches the behavior $w_{ma} \simeq w_{\mathrm{out}} = z - 1/2$, while the boundary layers (BL) become thinner and thinner. This points to the existence of the upper bound for the velocity variance, $\langle w^2 \rangle \leqslant \int_0^1 (z - 1/2)^2\, dz = 1/12$, which implies

$$\mathrm{Re} = \sqrt{\frac{\mathrm{Ra}}{\mathrm{Pr}}}\langle w^2 \rangle^{1/2} \leqslant \frac{1}{\sqrt{12}}\sqrt{\frac{\mathrm{Ra}}{\mathrm{Pr}}}. \tag{55}$$

A lower bound for Re can be obtained by just considering that the asymptotic outer solution is the one most contributing to the global velocity variance, so

$$\langle w^2 \rangle \gtrsim \int_\delta^{1-\delta} w_{\mathrm{out}}^2\, dz \simeq \int_\delta^{1-\delta} \left(z - \frac{1}{2}\right)^2 dz = \frac{(1-2\delta)^3}{12},$$

where δ is an estimation for the thickness of the kinetic boundary layer, which we define as the height z where the argument of the hyperbolic function in w_{in} is one, i.e., $\delta = 4/\sqrt{\mathrm{Ra/Pr}}$. This implies

$$\mathrm{Re} \gtrsim \frac{1}{\sqrt{12}}\sqrt{\frac{\mathrm{Ra}}{\mathrm{Pr}}}\left(1 - 8\sqrt{\frac{\mathrm{Pr}}{\mathrm{Ra}}}\right)^{3/2}. \tag{56}$$

We will show that the above predictions for the Nusselt and the Reynolds numbers approach quite well the result that we obtain from the numerical simulations of the BRB system in the asymptotic large-Ra limit (see below, Sec. IV C).

Scaling laws of the form $\mathrm{Nu} \sim \sqrt{\mathrm{Ra}\,\mathrm{Pr}}$ and $\mathrm{Re} \sim \sqrt{\mathrm{Ra}/\mathrm{Pr}}$ identify the so-called ultimate regime of thermal convection. Physically it can be interpreted as a regime where the microscopic diffusion material properties, i.e., the viscosity and the thermal diffusivities, have a negligible role in the determination of the intensity of the heat transport and of the kinetic energy in the system. The ultimate regime has been predicted to occur in the RB systems in the asymptotic high-Ra limit [27] (see also [28]). However, its verification in RB experiments and simulations is still debated (see [29] for a recent concise account). On the opposite, it has been clearly observed in the so-called homogeneous-Rayleigh-Benard (HRB) model system, which is a 3D vertically unbounded system, either triperiodic [14] or laterally confined [30], which can be realized only in numerical simulations. It is important to note that the HRB model has no horizontal wall boundaries, and as such it misses the corresponding kinetic and thermal boundary layers, i.e., well-identified regions where dissipation has the dominant role with respect to inertial transport terms. Experimental realizations of the $\mathrm{Nu} \sim \sqrt{\mathrm{Ra}}$ regime have been achieved only in bulk-dominated convective systems, such as in the vertical channel setup [31,32] or in systems where the wall thermal heating has been replaced by volumetric radiative heating [33,34]. More recently Ref. [35] numerically demonstrated the occurrence of the ultimate regime of convection also in a RB system with permeable walls. This system possesses thermal and kinetic BL but does not enforce the cancellation of the vertical velocity on the top-bottom walls. In light of this, the verification of Eqs. (54) and (55) for the BRB system in high-Ra regime would make it the first bounded system, with kinetic and thermal boundary layers, to display the ultimate regime. As we will numerically demonstrate in the next section, the BRB clearly possesses this feature.

IV. THE BRB DYNAMICS: NUMERICAL SIMULATION ANALYSIS

In order to test the predictions presented in the previous section and to get deeper insight into the BRB dynamics, we performed direct numerical simulations (DNS) of the system of equations. This is conveniently done by means of a Fourier pseudospectral method. For this study we use spatial resolutions ranging from $N = 2^{13}$ to 2^{16} grid points and explore the 2D parameter space Ra-Pr. The simulations evolve in time from an initial state where w and θ are null except for a tiny random uniform spatially uncorrelated perturbation. The adopted numerical methods and protocols are described in detail in the Appendix.

A. Temperature and velocity profiles

We numerically find that the system displays a steady solution at any Ra, up to 10^{10} simulated in this study, and at any Pr in the range $[10^{-2}, 10^{2}]$. Furthermore, when $\mathrm{Pr} = 1$ the w and θ profiles are always coincident. As illustrated in Figs. 3 and 4 when the Rayleigh number is slightly beyond the critical threshold $\mathrm{Ra} = O(10^3)$, the two-mode solution (31)–(32) perfectly approximates the numerically computed temperature and velocity profiles. On the other hand for $\mathrm{Ra} = 10^5$ the agreement with the matched asymptotic solution (49) is already excellent. It is also evident that as $\mathrm{Ra} \to +\infty$ the profiles approach the $z - 1/2$ linear shape, with vanishingly thin boundary layers. Note that the temperature T is the sum of the conductive profile and the fluctuation θ; this implies that T is essentially constant in the well-mixed bulk of the system and changes sharply only in the boundary layer, in close analogy with the mean vertical temperature profile in the turbulent high-Ra RB system.

Figure 4 reports the corresponding numerical results for nonunit Prandtl numbers ($\mathrm{Pr} = 5$ and $1/5$) at $\mathrm{Ra} = 10^5$. One can appreciate that for $\mathrm{Pr} > 1$ the thermal boundary layer is thinner than the kinetic one and vice versa for $\mathrm{Pr} < 1$. Note also that the two cases are distinct, because $\mathrm{Pr} \to \mathrm{Pr}^{-1}$ is not a symmetry of the system. Again we observe a good agreement with the matched asymptotic solutions (47)–(48). In the asymptotic high-Pr limit one shall expect that θ will become almost everywhere equal to $z - 1/2$, while in the low-Pr limit the same will happen for w.

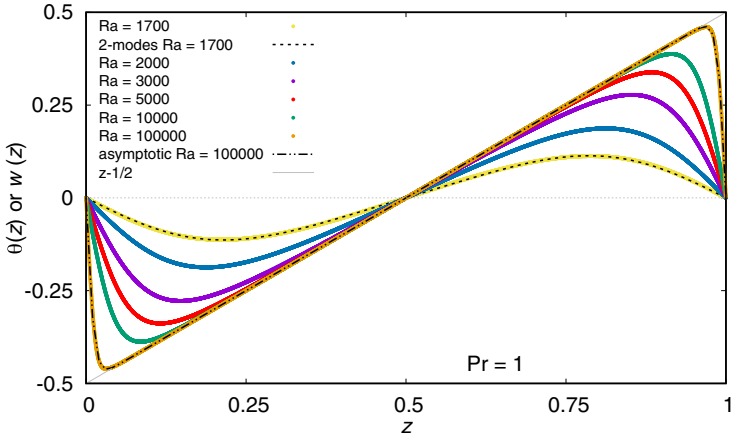

FIG. 3. Graph of the numerical solution for the temperature fluctuation $\theta(z)$ at $\mathrm{Pr} = 1$ [identical to the velocity $w(z)$] for several Ra values from $\mathrm{Ra} = 1700 = 1.09\mathrm{Ra}_c$ to $\mathrm{Ra} = 10^5 = 64.16\mathrm{Ra}_c$. The two-mode truncated solution for $\mathrm{Ra} = 1700$ is shown as well as the matched asymptotic one for $\mathrm{Ra} = 10^5$. The solution approaches the bulk behavior, $z - 1/2$, at increasing the Ra number.

B. Is the convective stationary regime stable?

As mentioned above, numerically we find that the convective state of the system displays a stationary solution at any Ra and Pr values. This aspect might seem surprising as it is different from what happens in the RB system, where successive bifurcations occur as Ra is increased, leading first to temporally periodic solutions, then chaotic ones, and finally to progressively more turbulent states. In the BRB case, although we cannot rule out the existence of subcritical bifurcations that might lead to the existence of such unsteady states, we can prove that the convective state displayed by the system is linearly stable. This point is addressed in the current section.

In Sec. III A we studied the stability of the conductive state. It was shown that, beyond $\mathrm{Ra}_c = k^4 = (2\pi)^4$, the system bifurcates to a convective stationary state, hereafter denoted as w_s, θ_s. Depending on the value of Ra this state can be approximated in three ways:

(i) By a two-mode expansion Eqs. (19) and (31)–(32), valid near the critical threshold Ra_c

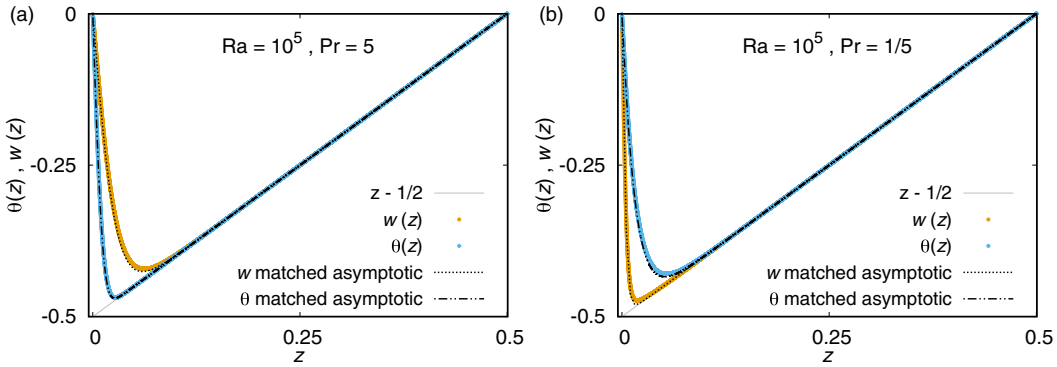

FIG. 4. Numerical solution for the temperature fluctuation $\theta(z)$ and velocity $w(z)$ at $\mathrm{Ra} = 10^5$ and $\mathrm{Pr} = 5$ (a) and $\mathrm{Pr} = 1/5$ (b), and comparison with the matched asymptotic solutions for both fields. Note that the profile is shown for better visibility only in the bottom half of the domain (the top part being its mirrored image).

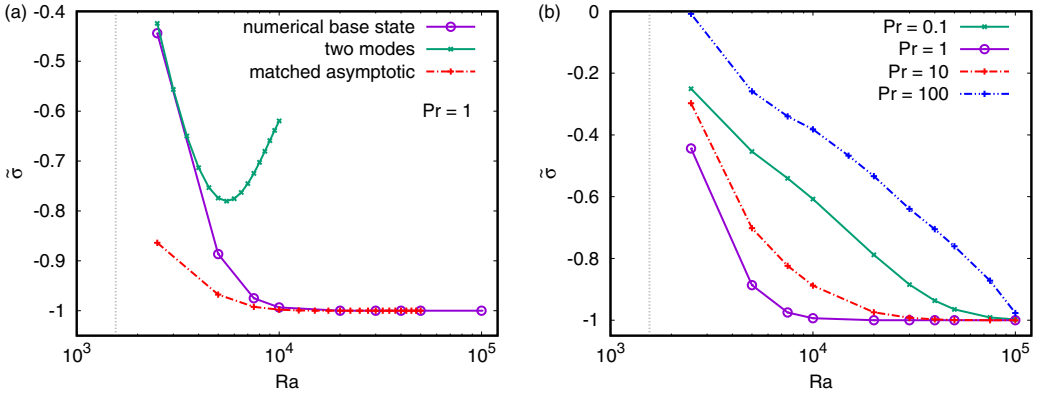

FIG. 5. Results of linear stability analysis of the convective steady state w_s, θ_s. Perturbation growth rate $\tilde{\sigma}$ as a function of Ra: (a) for the case $\mathrm{Pr} = 1$ computed from three different representations of the base state: the numerical (valid in the full range of Ra), the two-mode Galerkin truncation base state (valid at small Ra), and the matched asymptotic one (valid for $\mathrm{Ra} \to +\infty$); (b) for different Prandtl numbers $\mathrm{Pr} \in [0.1, 10^2]$ using the numerical base state. The dotted vertical line is traced at $\mathrm{Ra} = \mathrm{Ra}_c$.

(ii) By a matched asymptotic solution Eqs. (47)–(48), valid in the limit of large Rayleigh numbers

(iii) By an interpolation of the discretized numerical solution obtained from the DNS, which is valid in the whole Ra range.

We can now study the stability of these states by applying the linear stability analysis. We adopt the Galerkin method of weighted residuals [36]. In short, the idea is to choose trial functions that satisfy the boundary conditions exactly and solve the differential equations in an averaged sense, by imposing the condition that the residuals are orthogonal to the trial functions. The result is a set of homogeneous equations whose nontrivial solution leads to an eigenvalue problem. We denote with $\tilde{\sigma}(n)$ the series of the eigenvalues, which are determined in terms of the Ra and Pr parameters. Similarly to the previous case, we write

$$w = \sum_{n=1}^{N} \tilde{w}_n \sin(nkz) e^{\tilde{\sigma}(n)t} + w_s, \quad \theta = \sum_{n=1}^{N} \tilde{\theta}_n \sin(nkz) e^{\tilde{\sigma}(n)t} + \theta_s \tag{57}$$

with $n \in \mathbb{N}$ and $k = 2\pi$. The number of modes N is chosen so that the convergence is ensured for the different parameter values.

Figure 5(a) shows the evolution of the perturbation growth rate $\tilde{\sigma} = \tilde{\sigma}(1)$ with $\mathrm{Ra}(> \mathrm{Ra}_c)$, for the three different approximated base solutions and $\mathrm{Pr} = 1$. As expected, the two-mode solution (case 1) agrees well with the numerical convective state (case 3) for moderate values of the Rayleigh number, while the matched asymptotic does it for large values. The evolution of the larger growth rate $\tilde{\sigma}$ for different values of Prandtl obtained with the numerical base state is depicted in Fig. 5(b). It can be seen that the growth rate is always negative, indicating that the the first convective stationary state never loses its stability, even for large values of Ra, in agreement with the observations from the DNS.

C. Measure of Nusselt and Reynolds number asymptotic scalings

Form the numerically computed $\theta(z)$ and $w(z)$ profiles one can estimate the corresponding Nusselt and Reynolds numbers and analyze their functional dependencies with Ra and Pr.

The behavior of Nu as a function of Ra, for $\mathrm{Pr} = 1$, is shown in Fig. 6(a). We observe that for $\mathrm{Ra} < \mathrm{Ra}_c$ $\mathrm{Nu} \simeq 1$ (vertical dotted line), hence only conductive heat-transfer occurs, as expected

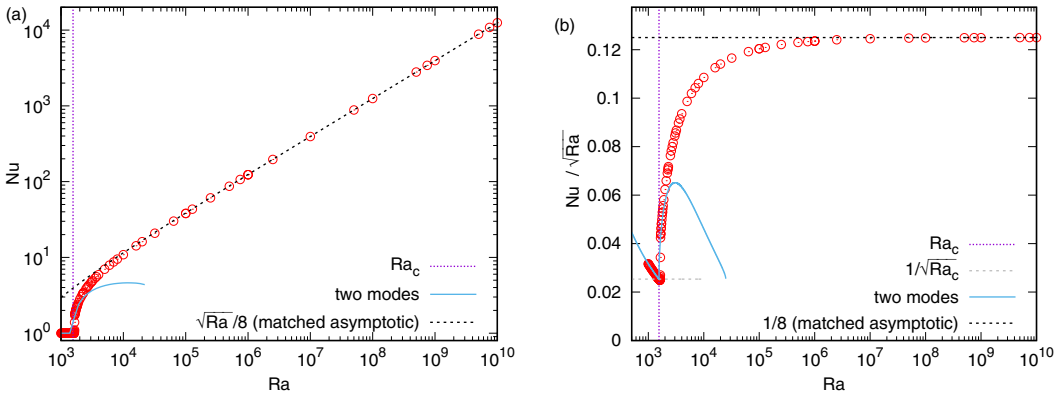

FIG. 6. Nusselt-Rayleigh scaling at $\mathrm{Pr} = 1$. (a) Nu vs Ra. Numerical simulation results (red circle symbols) and comparisons with different analytical predictions: (vertical dotted line) the critical Rayleigh number for the onset of convection $\mathrm{Ra}_c \simeq 1558$; (solid line) the Nusselt number calculated from the two-mode steady solution (33); and (dashed line) the Nu expression computed via the matched asymptotic solution $\mathrm{Nu} = \sqrt{\mathrm{Ra}}/8$. (b) The same data points for Nu and theoretical predictions, compensated with respect to $\mathrm{Ra}^{1/2}$.

from the theoretical analysis. Beyond Ra_c convection starts and Nu progressively increases. Close to the onset, for $\mathrm{Ra} \lesssim 2\mathrm{Ra}_c \sim 3 \times 10^3$, the two-mode expression (33) (solid line) approaches well the numerical results. On the other hand the matched asymptotic prediction agrees with the data from $\mathrm{Ra} \sim 10^4$ (dashed line) up to the highest explored Ra number (10^{10}). Indeed, as is better appreciated in the compensated plot Fig. 6(b) at the largest Ra the normalized data approach the value $1/8$ (dashed-dotted line) meaning that $\mathrm{Nu} \sim \sqrt{\mathrm{Ra}}/8$ in excellent agreement with the *ma* prediction (54).

We now look at the heat-flux dependence with respect to Pr. This is illustrated in Fig. 7(a), where Nu(Pr) is traced for various Rayleigh numbers $\mathrm{Ra} = 10^6, 10^7, 10^8$. Also in this case we see an excellent agreement with the matched asymptotic solution (50) and with the small- and large-Pr asymptotic behaviors (52)–(53) derived in the previous section. We clearly observe a saturation of the Nusselt number for $\mathrm{Pr} \gg 1$. Furthermore, Fig. 7(b) shows how all the data points can be collapsed on a single curve, by means of the rescaling $\mathrm{Nu}/\sqrt{\mathrm{Ra}}$. This means that, in agreement with the matched asymptotic solution, the Ra and Pr dependence can be factorized [see Eq. (51)].

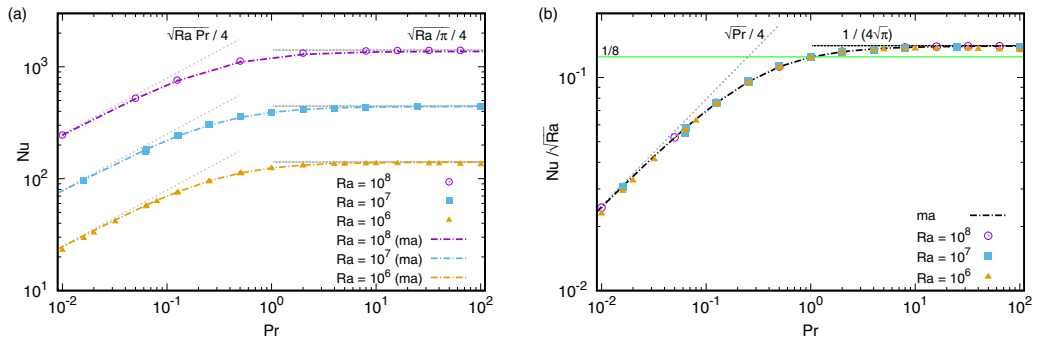

FIG. 7. Nusselt-Prandlt scaling behavior at various Rayleigh numbers $\mathrm{Ra} = 10^6, 10^7, 10^8$. (a) Nusselt as a function of Prandtl. We display the numerical simulation results (symbols) and the corresponding matched asymptotic predictions (colored dotted-dashed lines). The behaviors $\sqrt{\mathrm{RaPr}}/4$ for small Pr (graydashed line) and $\sqrt{\mathrm{Ra}/\pi}/4$ for large Pr (black dotted line). (b) Compensated graph $\mathrm{Nu}/\sqrt{\mathrm{Ra}}$ vs Pr. The value $1/8$ corresponding to $\mathrm{Pr} = 1$ is also traced. One can appreciate the collapse of the measurements on a single curve.

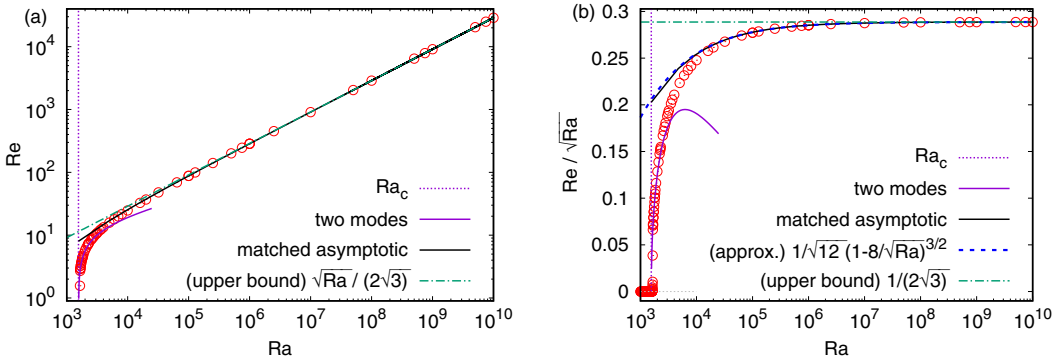

FIG. 8. Reynolds-Rayleigh scaling at $\mathrm{Pr} = 1$. (a) Re vs Ra. The numerical simulation results (red circle symbols) and comparisons with different analytical predictions: (vertical dotted line) the critical Rayleigh number for the onset of convection $\mathrm{Ra}_c \simeq 1558$; (violet solid line) the Reynolds number calculated from the two-mode steady solution (35); (black solid line) the Re expression computed via the matched asymptotic solution; and (green dotted-dashed line) the upper bound value $\mathrm{Re} = \sqrt{\mathrm{Ra}/12}$ [Eq. (55)]. (b) The same data points for Re and theoretical predictions, here compensated with respect to $\mathrm{Ra}^{1/2}$ We include also the approximated expression (56) (blue dashed line), which has a much simpler form as the *ma* prediction and fits equally well the measurements at large Ra.

Similar observations can be made for the dependence of the Reynolds number versus Ra for $\mathrm{Pr} = 1$ [Figs. 8(a) and 8(b)] and Re(Pr) Fig. 9(a)]. At high Ra agreement with the *ma* predictions is satisfactory in all cases. The Re(Ra, Pr) functional relation is also well described by the expression (56), which is simpler in form than the *ma* expression [see again Fig. 8(b) and Fig. 9(a)]. In Fig. 9(a) we observe that the compensated Reynolds number expression $\mathrm{Re}/\sqrt{\mathrm{Ra}/\mathrm{Pr}}$, which is equivalent to the mean root-mean-squared velocity $\sqrt{\langle w^2 \rangle}$, decreases for large Pr. This is consistent with the fact that the kinematic boundary layer becomes thicker, hence the velocity reduce in intensity. The opposite is true for the fluctuations of the temperature field $\sqrt{\langle \theta^2 \rangle}$, which is reported in Fig. 9(b), and for which again the *ma* solution offers an excellent approximation.

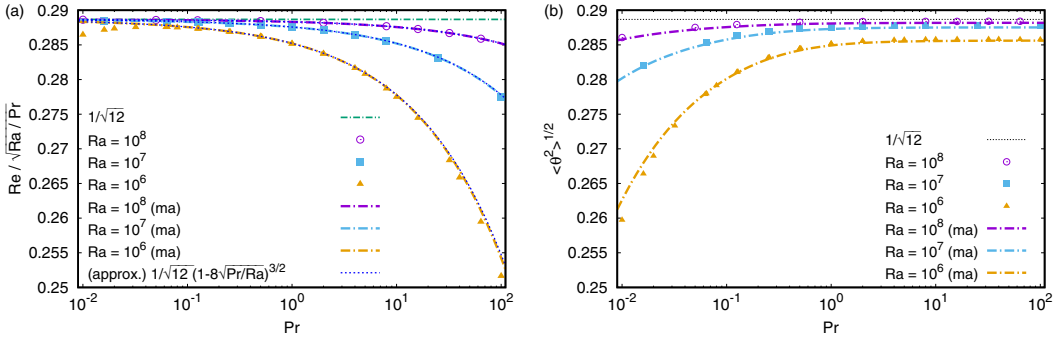

FIG. 9. Reynolds number scaling vs Pr. (a) Compensated Reynolds number $\mathrm{Re}/\sqrt{\mathrm{Ra}/\mathrm{Pr}}$, equivalent to the root-mean-square value of the velocity $\sqrt{\langle w^2 \rangle}$ as a function of $\mathrm{Pr} \in [10^{-2}, 10^2]$ for $\mathrm{Ra} = 10^6, 10^7, 10^8$; (b) root-mean-square value of the temperature fluctuation $\sqrt{\langle \theta^2 \rangle}$. In both cases the numerical simulation results (symbols) and comparisons with the dependencies computed upon integration of the matched asymptotic solutions (47) and (48) and the upper bound $1/\sqrt{12}$ (green dashed-dotted) that can be computed from the bulk solution. In (a) the algebraic approximation (56) (dotted) is also reported.

Overall the DNS confirms the realization of the ultimate regime for the Reynolds and Nusselt numbers in respect to both the Rayleigh and Prandtl dependence. To our knowledge the occurrence of this regime was previously assessed only for the 3D homogeneous-Rayleigh-Bénard system in [14] and more recently in a wider Ra and Pr range in [37]. Despite its great degree of abstraction (1D, compressible flow) the BRB system represents a second convective model system where this flow regime takes place. Moreover the saturation of Nu for large-Pr is a feature of the RB model [8], which is present here, while it was missing in the HRB system.

V. CONCLUSIONS

The BRB dynamics shares remarkable similarities with realistic thermal convection in higher spatial dimensions, i.e., the Rayleigh-Bénard system under Oberbeck-Boussinesq conditions. In this work we have shown that (1) BRB has a supercritical linear instability for the onset of convection which solely depends on the Rayleigh number and not on the Prandlt number (the same as in RB), occurring at the critical value $\mathrm{Ra}_c \approx 1558$, which is of the same order as in the RB system; (2) the convective regime is spatially organized in distinct boundary layers and bulk regions, although shocklike solutions are equally admitted; and (3) the asymptotic high Ra limit displays the ultimate Nusselt and Reynolds number scaling regime $\mathrm{Nu} = \sqrt{\mathrm{RaPr}}/4$ for $\mathrm{Pr} \ll 1$, $\mathrm{Nu} = \sqrt{\mathrm{Ra}}/(4\sqrt{\pi})$ for $\mathrm{Pr} \gg 1$ and $\mathrm{Re} = \sqrt{\mathrm{Ra}/\mathrm{Pr}}/\sqrt{12}$ thus making BRB the simplest convective system with boundaries exhibiting the ultimate regime of convection. A major difference with realistic higher-dimensional natural convection is the absence of turbulence. The BRB dynamics is stationary at all Ra numbers above the onset of convection for all Pr values, a feature that results from a nonlinear saturation mechanism.

One may object that the odd symmetry in w and θ makes the BRB *de facto* a periodic system, as the fields can be expressed in term of sine series. For this reason in the future it would be interesting to explore the dynamics of this system in a higher (two- or three-) dimensional space. In this case, the convective state might be unstable due to the larger number of degrees of freedom and to the increased system symmetries available in higher dimensions.

Whether the missing physics in the present model, namely, the violation of the incompressibility or the absence of the pressure field or of the spatial lateral dimensions, might be related to the realization of the ultimate regime of heat transfer remains a question for further investigations. In this sense it would be interesting, and perhaps useful, to think of a similar minimalist model capable of reproducing the classical scaling of thermal convection ($\mathrm{Nu} \sim \mathrm{Ra}^{1/3}$), in order to see which key mathematical terms and corresponding physical features are needed for the realization of this different convection regime.

The codes used in this study are available at [38].

ACKNOWLEDGMENT

The authors are grateful to Prof. M. N. Ouarzazi for useful comments.

APPENDIX: NUMERICAL SIMULATION METHOD

Equations (6)–(7) in Fourier space, denoted with a tilde ($\tilde{}$), read

$$\tilde{w}_t + \widetilde{w w_z} = -k^2 \sqrt{\frac{\mathrm{Pr}}{\mathrm{Ra}}}\, \tilde{w} + \tilde{\theta}, \tag{A1}$$

$$\tilde{\theta}_t + \widetilde{w\theta_z} = -k^2 \frac{1}{\sqrt{\mathrm{PrRa}}} \tilde{\theta} + \tilde{w}. \tag{A2}$$

The dissipative terms can be analytically integrated, while the nonlinear terms can be evaluated via a pseudospectral algorithm. In our code we adopt the standard two-thirds dealiasing procedure for the

computation of the nonlinear terms. Furthermore, we enforce the boundary conditions by imposing that both w and θ are in real space zero-mean odd functions (i.e., we use the sine transform instead of Fourier). The temporal discretization with time step δt, performed by means of a second-order Adams-Bashfort algorithm, leads to

$$\tilde{w}_{n+1} = \left\{ \tilde{w}_n + \frac{\delta t}{2}(3[-\widetilde{w w}_z + \tilde{\theta}]_n - [-\widetilde{w w}_z + \tilde{\theta}]_{n-1} e^{-k^2 \sqrt{\frac{\mathrm{Pr}}{\mathrm{Ra}}} \delta t}) \right\} e^{-k^2 \sqrt{\frac{\mathrm{Pr}}{\mathrm{Ra}}} \delta t}, \tag{A3}$$

$$\tilde{\theta}_{n+1} = \left\{ \tilde{\theta}_n + \frac{\delta t}{2}(3[-\widetilde{w\theta}_z + \tilde{w}]_n - [-\widetilde{w\theta}_z + \tilde{w}]_{n-1} e^{-k^2 \frac{1}{\sqrt{\mathrm{PrRa}}} \delta t}) \right\} e^{-k^2 \frac{1}{\sqrt{\mathrm{PrRa}}} \delta t}, \tag{A4}$$

where the subscript indexes indicate the discretized value of time. The time step width is chosen as $\delta t = 10^{-2}/\sigma$, where σ is the growth rate of the most unstable mode, Eq. (18), while the spatial resolution is increased till when the resulting velocity and temperature profiles become independent on the number of discretization points N. However, we note that the existence of sharp variations in the solution is at odds with our discretization method based on sine-Fourier transform, which is known for being affected by the Gibbs phenomenon. Indeed, at high-Ra some Gibbs-like spurious fluctuations are seen in correspondence of the bulk to boundary layer transition. This fluctuations do not affect the scaling laws presented in this work. The simulations of the BRB system have been also validated against a second code based on finite-difference discretization.

The temperature and velocity fields in the simulations are initialized with a spatially uncorrelated pseudorandom noise. These perturbations lead in 50% of cases to the BL-type solution and in the remaining cases to the shock solution. Although these two states correspond to different global heat-transfer modes, the resulting velocity and temperature profiles can be transformed one into another by the swap transformation, Eq. (8). In the present analysis, focused on the scaling of Nusselt in the BL-type state, we take advantage of the swap transformation to maximize the the number of realizations of BL solutions. However, we note that it is possible to direct the instability towards one of the two possible convective states, e.g., by adding a sinusoidal modulation to the initial white noise. A modulation of the form $-\sin(2\pi z)$ leads to BL state, while its opposite, $\sin(2\pi z)$, favors the transition towards the shock-type solution. This aspect has an analogous in the RB system where one can control the large-scale circulation direction of the convective cells by initializing the flow with an horizontally asymmetric perturbation of the temperature field.

[1] E. N. Lorenz, Deterministic nonperiodic flow, J. Atmos. Sci. **20**, 130 (1963).

[2] E. B. Gledzer, System of hydrodynamic type admitting two quadratic integrals of motion, Dokl. Akad. Nauk SSSR **209**, 1046 (1973).

[3] K. Ohkitani and M. Yamada, Temporal intermittency in the energy cascade process and local Lyapunov analysis in fully developed model of turbulence, Prog. Theor. Phys. **81**, 329 (1989).

[4] Y. Du, H. Li, and L. P. Kadanoff, Breakdown of Hydrodynamics in a One-Dimensional System of Inelastic Particles, Phys. Rev. Lett. **74**, 1268 (1995).

[5] P. Eshuis, K. van der Weele, E. Calzavarini, D. Lohse, and D. van der Meer, Exploring the limits of granular hydrodynamics: A horizontal array of inelastic particles, Phys. Rev. E **80**, 011302 (2009).

[6] F. L. Rayleigh, On convection currents in a horizontal layer of fluid, when the higher temperature is on the under side, London Edinburgh Dublin Philosoph. Mag. J. Sci. **32**, 529 (1916).

[7] A. Getling, *Rayleigh-Benard Convection: Structures and Dynamics* (World Scientific, Singapore, 1998).

[8] G. Ahlers, S. Grossmann, and D. Lohse, Heat transfer and large scale dynamics in turbulent Rayleigh-Bénard convection, Rev. Mod. Phys. **81**, 503 (2009).

[9] J. M. Burgers, A mathematical model illustrating the theory of turbulence, Adv. Appl. Mech. **1**, 171 (1948).

[10] E. Hopf, The partial differential equation: $u_t + uu_x = \epsilon u_{xx}$, Comm. Pure Appl. Math. **3**, 201 (1950).

[11] J. D. Cole, On a quasi-linear parabolic equation occurring in aerodynamics, Q. Appl. Math. **9**, 225 (1951).

[12] U. Frisch and J. Bec, Burgulence, in *New Trends in Turbulence Turbulence: Nouveaux Aspects: 31 July–1 September 2000*, edited by M. Lesieur, A. Yaglom, and F. David (Springer, Berlin, 2001), pp. 341–383.
[13] J. Bec and K. Khanin, Burgers turbulence, Phys. Rep. **447**, 1 (2007).
[14] E. Calzavarini, D. Lohse, F. Toschi, and R. Tripiccione, Rayleigh and Prandtl number scaling in the bulk of Rayleigh–Bénard turbulence, Phys. Fluids **17**, 055107 (2005).
[15] E. Calzavarini, C. R. Doering, J. D. Gibbon, D. Lohse, A. Tanabe, and F. Toschi, Exponentially growing solutions in homogeneous Rayleigh-Bénard convection, Phys. Rev. E **73**, 035301(R) (2006).
[16] L. D. Landau and E. M. Lifshitz, *Fluid Mechanics, Volume 6, Course of Theoretical Physics*, 2nd ed. (Butterworth-Heinemann, Oxford, 1987).
[17] The stability of the three fixed points can be also assessed by means of the analysis of the eigenvalues of the Jacobian of the system of equations (24) and (25), and in particular their dependence with respect to the control parameter Ra. This leads to the fact that the equilibrium point $A_1 = A_2 = 0$ changes from stable to unstable when $\mathrm{Ra} > \mathrm{Ra}_c$, while the two fixed points (31) and (32) become stable as long as $\mathrm{Ra}_c < \mathrm{Ra} < 16\mathrm{Ra}_c$. This identifies a supercritical pitchfork bifurcation; see Fig. 2.
[18] C. M. Orszag and S. A. Bender, *Advanced Mathematical Methods for Scientists and Engineers I: Asymptotic Methods and Perturbation Theory* (Springer, New York, NY, 1999).
[19] J. Goodman and Z. Xin, Viscous limits for piecewise smooth solutions to systems of conservation laws, Arch. Rational Mech. Anal. **121**, 235 (1992).
[20] J. P. Boyd, The energy spectrum of fronts: time evolution of shocks in Burgers' equation, J. Atmos. Sci. **49**, 128 (1992).
[21] E. Weinan and E. Vanden Eijnden, Asymptotic Theory for the Probability Density Functions in Burgers Turbulence, Phys. Rev. Lett. **83**, 2572 (1999).
[22] G. L. Eyink and T. D. Drivas, Spontaneous stochasticity and anomalous dissipation for Burgers equation, J. Stat. Phys. **158**, 386 (2015).
[23] M. Van Dyke, *Perturbation Methods in Fluid Mechanics* (Parabolic Press, Stanford, CA, 1975).
[24] P. G. Saffman, Lectures on homogeneous turbulence, in *Topics in Nonlinear Physics*, edited by N. J. Zabusky (Springer, Berlin, 1968), pp. 485–614.
[25] S. Alam, P. K. Sahu, and M. K. Verma, Universal functions for Burgers turbulence, Phys. Rev. Fluids **7**, 074605 (2022).
[26] R. J. A. M. Stevens, E. P. van der Poel, S. Grossmann, and D. Lohse, The unifying theory of scaling in thermal convection: The updated prefactors, J. Fluid Mech. **730**, 295 (2013).
[27] R. H. Kraichnan, Turbulent thermal convection at arbitrary Prandtl number, Phys. Fluids **5**, 1374 (1962).
[28] S. Grossmann and D. Lohse, Scaling in thermal convection: A unifying theory, J. Fluid Mech. **407**, 27 (2000).
[29] C. Doering, Turning up the heat in turbulent thermal convection, Proc. Natl. Acad. Sci. USA **117**, 9671 (2020).
[30] L. E. Schmidt, E. Calzavarini, D. Lohse, F. Toschi, and R. Verzicco, Axially homogeneous Rayleigh–Bénard convection in a cylindrical cell, J. Fluid Mech. **691**, 52 (2012).
[31] M. Gibert, H. Pabiou, F. Chillà, and B. Castaing, High-Rayleigh-Number Convection in a Vertical Channel, Phys. Rev. Lett. **96**, 084501 (2006).
[32] M. R. Cholemary and J. H. Arakeri, Axially homogeneous, zero mean flow buoyancy-driven turbulence in a vertical pipe, J. Fluid Mech. **621**, 69 (2009).
[33] S. Lepot, S. Aumaitre, and B. Gallet, Radiative heating achieves the ultimate regime of thermal convection, Proc. Natl. Acad. Sci. USA **115**, 8937 (2018).
[34] V. Bouillaut, S. Lepot, S. Aumaître, and B. Gallet, Transition to the ultimate regime in a radiatively driven convection experiment, J. Fluid Mech. **861**, R5 (2019).
[35] K. Kawano, S. Motoki, M. Shimizu, and G. Kawahara, Ultimate heat transfer in 'wall-bounded' convective turbulence, J. Fluid Mech. **914**, A13 (2021).
[36] B. A. Finlayson, *The Method of Weighted Residuals and Variational Principles* (Academic Press, 1972).
[37] A. Barral and B. Dubrulle, Asymptotic ultimate regime of homogeneous Rayleigh–Bénard convection on logarithmic lattices, J. Fluid Mech. **962**, A2 (2023).
[38] https://github.com/ecalzavarini/BurgersRB.